MOLECULAR
METABOLISM

Changes in liver metabolic pathways demonstrate efficacy of the combined dietary and microbial therapeutic intervention in MASLD mouse model

Valeria Iannone [1,12], Ambrin Farizah Babu [1,2,12], Johnson Lok [1], Carlos Gómez-Gallego [1,*], Giuseppe D'Auria [3,4], Ruben Vazquez-Uribe [5], Troels Holger Vaaben [5], Mareike Bongers [5], Santtu Mikkonen [6], Maija Vaittinen [1], Ida Tikkanen [1], Mikko Kettunen [7], Anton Klåvus [2], Ratika Sehgal [1], Dorota Kaminska [1,8], Jussi Pihlajamaki [1,9], Kati Hanhineva [1,2,10,13], Hani El-Nezami [1,11,13], Morten Otto Alexander Sommer [5,**,13], Marjukka Kolehmainen [1,13]

ABSTRACT

Objective: Metabolic dysfunction-associated steatotic liver disease (MASLD), formerly known as non-alcoholic fatty liver disease (NAFLD), is the most prevalent liver disease globally, yet no therapies are approved. The effects of *Escherichia coli* Nissle 1917 expressing aldafermin, an engineered analog of the intestinal hormone FGF19, in combination with dietary change were investigated as a potential treatment for MASLD.
Methods: MASLD was induced in C57BL/6J male mice by American lifestyle-induced obesity syndrome diet and then switched to a standard chow diet for seven weeks. In addition to the dietary change, the intervention group received genetically engineered *E. coli* Nissle expressing aldafermin, while control groups received either *E. coli* Nissle vehicle or no treatment. MASLD-related plasma biomarkers were measured using an automated clinical chemistry analyzer. The liver steatosis was assessed by histology and bioimaging analysis using Fiji (ImageJ) software. The effects of the intervention in the liver were also evaluated by RNA sequencing and liquid-chromatography-based non-targeted metabolomics analysis. Pathway enrichment studies were conducted by integrating the differentially expressed genes from the transcriptomics findings with the metabolites from the metabolomics results using Ingenuity pathway analysis.
Results: After the intervention, *E. coli* Nissle expressing aldafermin along with dietary changes reduced body weight, liver steatosis, plasma aspartate aminotransferase, and plasma cholesterol levels compared to the two control groups. The integration of transcriptomics with non-targeted metabolomics analysis revealed the downregulation of amino acid metabolism and related receptor signaling pathways potentially implicated in the reduction of hepatic steatosis and insulin resistance. Moreover, the downregulation of pathways linked to lipid metabolism and changes in amino acid-related pathways suggested an overall reduction of oxidative stress in the liver.
Conclusions: These data support the potential for using engineered microbial therapeutics in combination with dietary changes for managing MASLD.

[1]School of Medicine, Institute of Public Health and Clinical Nutrition, University of Eastern Finland, 70200 Kuopio, Finland [2]Afekta Technologies Ltd., Microkatu 1, 70210 Kuopio, Finland [3]Sequencing and Bioinformatics Service, Foundation for the Promotion of Health and Biomedical Research of Valencia Region, FISABIO, 46020 Valencia, Spain [4]CIBER in Epidemiology and Public Health (CIBERESP), Instituto de Salud Carlos III, 28029, Madrid, Spain [5]Technical University of Denmark, The Novo Nordisk Foundation Center for Biosustainability, 2800 Kongens Lyngby, Denmark [6]University Department of Technical Physics, University of Eastern Finland, 70211 Kuopio, Finland [7]Biomedical Imaging Unit, A.I. Virtanen Institute for Molecular Sciences, University of Eastern Finland, 70211, Kuopio, Finland [8]Department of Medicine, Division of Cardiology, University of California, Los Angeles, CA 90095, USA [9]Department of Medicine, Endocrinology and Clinical Nutrition, Kuopio University Hospital, 70210 Kuopio, Finland [10]Department of Life Technologies, Food Sciences Unit, University of Turku, 20014 Turku, Finland [11]University of Hong Kong, Hong Kong SAR, Molecular and Cell Biology Research Area, School of Biological Sciences, Hong Kong, Hong Kong, China

[12] Equal contributions.

[13] Equal contributions.

*Corresponding author. Institute of Public Health and Clinical Nutrition, University of Eastern Finland, Mediteknia, h. 4042, Yliopistonranta 1 B, 70210 Kuopio, Finland. E-mail: carlos.gomezgallego@uef.fi (C. Gómez-Gallego).

**Corresponding author. Technical University of Denmark, The Novo Nordisk Foundation Center for Biosustainability, Kongens Lyngby, Denmark. E-mail: msom@bio.dtu.dk (M.O.A. Sommer).

Original Article

1. INTRODUCTION

A healthy diet and increased physical activity are the predominant interventions in the treatment of metabolic dysfunction-associated steatotic liver disease (MASLD), previously known as non-alcoholic fatty liver disease (NAFLD), which is the most common liver disease worldwide [1]. Despite its prevalence, no medical treatments for MASLD have been approved.

Furthermore, despite ongoing research, our understanding of MASLD pathogenesis remains limited [2]. Briefly, the role of insulin resistance (IR) exacerbating fat accumulation in the liver during the disease development has been well established [3]. Moreover, the excessive fatty acid oxidation [4] and impairment of triglyceride accumulation [5,6] in the liver plays a crucial role in the accumulation of toxic lipids [2,6]. Consequently, lipotoxicity induces detrimental effects such as oxidative stress, contributing to the progression of MASLD to metabolic dysfunction-associated steatohepatitis (MASH; formerly known as nonalcoholic steatohepatitis, NASH) [2]. Patients with MASLD often have an impaired intestinal fibroblast growth factor 19 (FGF19) production [7], a regulator of lipid and energy metabolism in the liver [8]. Previous studies have shown that administration of FGF19 to mice fed with a high-fat diet (HFD) can ameliorate the metabolic phenotype [9]. However, due to its tumorigenicity [10], the use of aldafermin, a non-tumorigenic analog of FGF19 has been recommended as a safer alternative treatment for MASLD [10,11]. Beneficial effects of aldafermin intervention have been observed in MASH patients, including reduced liver fat accumulation, liver enzyme levels such as alanine aminotransferase (ALT) and aspartate amino transferase (AST) in the plasma, and serum levels of bile acids [12]. However, the effects of aldafermin and its mechanism of action during the early MASLD stage remain to be investigated.

The gut microbiome is increasingly recognized to play an important role in the development and progression of MASLD [13–15]. Emerging research suggests that targeting the gut microbiome with probiotics, prebiotics, and other interventions may hold promise as a therapeutic approach for MASLD [15]. Indeed, the non-pathogenic gram-negative *Escherichia coli* Nissle 1917 has emerged as a potential therapeutic candidate for MASLD, demonstrating promising results in inhibiting MASLD progression in rats [16]. The use of advanced microbial therapeutics that are probiotics engineered to express a programmed therapeutic activity represents a promising strategy to manage MASLD and other metabolic diseases. Indeed, recent studies have used genetically engineered *E. coli* Nissle 1917 to deliver bioactive molecules to induce beneficial effects in metabolic disturbances, including obesity [17,18].

In this study, it was hypothesized that a multi-targeted intervention utilizing genetically engineered *E. coli* Nissle expressing aldafermin in combination with dietary change (EcNA) may offer an effective approach to manage MASLD-induced symptoms. Transcriptomics and non-targeted metabolomic techniques were employed to study the impact of EcNA in a mouse model of MASLD. The findings showed substantial alterations in hepatic metabolism and genes upon the administration of EcNA, indicating its potential as an innovative therapeutic for MASLD.

2. MATERIAL AND METHODS

2.1. *E. coli* Nissle 1917 strain engineering to express aldafermin

Aldafermin was constitutively expressed in a pMUT-1-based plasmid native to *E. coli* Nissle, using the strongest promoter from the Schantzetta library [19], designed for stable expression in the murine gastrointestinal tract. Briefly, the aldafermin gene was ordered as a gBlock (Integrated DNA Technologies) and amplified with uracil-containing primers using Phusion U Hot Start DNA Polymerase (ThermoFisher, Waltham, Massachusetts, United States, Cat No. F555S). Purified polymerase chain reaction fragments were treated with 0.5 μL of USER enzyme (NEB) in $1\times$ Cut Smart buffer (NEB) and subsequently incubated for 30 min at 37 °C in a thermocycler and 1 h at room temperature. Two μL of USER mixture was then used to transform One Shot™ TOP10 Chemically Competent *E. coli* (Thermofisher, Waltham, Massachusetts, United States) according to the instruction of the supplier (One Shot™ TOP10 Thermo Fisher, Waltham, Massachusetts, United States). Transformed cells were plated on selective culture media, and colonies were verified with colony polymerase chain reaction and subsequent sequencing. A positive colony was inoculated into 2 mL of Luria—Bertani with 50 μg/mL kanamycin and grown for 16 h, after which the plasmid was extracted using a NucleoSpin Plasmid EasyPure extraction kit (Macherey Nagel). Purified plasmid was used to transform electrocompetent cells of *E. coli* Nissle (Tn7:sfGFP+, StrepR) by electroporation. sfGFP was integrated in the genome in an attTn7 attachment site at position 2672041 to 2672355, expressed from the BBa_J23101 promoter (Additional file: Supplemental Figure S1). The strain of *E. coli* Nissle has previously been cured for any native pMUT1 plasmid.

2.2. *In vitro* production and strain characterization

For each strain, individual colonies were inoculated in 3 mL of Luria—Bertani media containing 100 μg/mL streptomycin and 50 μg/mL kanamycin and were then incubated at 37 °C overnight in a shaker at 200 rpm overnight. The following day, the cultures were diluted 100-fold in Greiner CELLSTAR 96-well microtiter plates (Sigma-Aldrich product number M0812) containing Luria—Bertani, 100 μg/mL streptomycin, and 50 μg/mL kanamycin, resulting in a final working volume of 200 μL. The plate was sealed using a BreathEasy film (Sigma-Aldrich, St. Louis, MO, USA) and was incubated in a Synergy H1 plate reader (BioTek, Winooski, VT, USA) at 37 °C and 1000 rpm. OD600 was measured every 5 min for 24 h. At the end of the fermentation, aliquots of the culture were collected and then centrifuged at $10,000 \times g$ for 5 min. The supernatant was collected and stored at −20 °C for later analysis. The samples were subjected to FGF19/aldafermin analysis by enzyme-linked immunosorbent assay (ELISA) following the manufacturer's protocol (Abcam: ab230943, Cambridge, United Kingdom).

To measure the growth rate of *E. coli* strains, 1:100 from an overnight culture grown in Luria Bertani at 37 °C was inoculated into 100 μL of liquid Luria Bertani media. The cultures were grown in 96-well microtiter plates at 37 °C with orbital shaking at 365 cpm (2 mm). A microtiter reader (BioTek ELx800) was used to measure the cell density every 5 min at optical density 600 nm (OD600). The growth rates were calculated by plotting the log OD measurements in the log phase and determining the slopes for time points in the log phase where the r^2 value was closest to 1. At least 24 time points (2 h apart) were used for the calculations.

2.3. Preparation of *E. coli* Nissle 1917 strains in gelatine cubes

The *E. coli* Nissle strains (with or without expression of aldafermin) were grown overnight at 37 °C and 200 rpm in Luria—Bertani broth with 100 μg/mL streptomycin + 50 μg/mL kanamycin. The next day, the cells were centrifugated for 10 min at 4000 rpm and the pellets were washed with 3 mL 0.9% saline solution twice. One hundred μL of the overnight culture was then added to a Luria—Bertani agar plate (without antibiotics) and incubated at 37 °C overnight. The next day, the bacteria were harvested by adding 1 mL of 10% sweetener ("Hermesetas Crunchy", Zurich, Switzerland) in tap water to the plate. To prepare the gelatine cubes, 20% of gelatine from "Dr. Oetker Gelatinpulver" (Bielefeld, Germany) were mixed in stock sweetener from "Hermesetas Crunchy" (Zurich, Switzerland). Vanilla flavoring from "Dr. Oetker Vanilla aroma" (Bielefeld, Germany) was added in a 70:5 ratio. Lastly, 75 μL of the bacterial culture was mixed with 75 μL of the gelatine stock in a 96-well plate and the plate was stored at 4 °C until *E. coli* Nissle administration. The next day, the concentration of 10^9 colony forming units (CFU) per cube of *E. coli* Nissle was confirmed by plating onto a Luria—Bertani agar plate with 50 μg/mL streptomycin + 50 μg/mL kanamycin.

2.4. Animal study

The experimental protocol for the use of mouse model was approved by the National Ethics Committee for Animal Experiments in Finland (license number: ESAVI/21371/2019) and conformed to the regulations and requirements of the European Union concerning the protection of animals used for scientific purposes. Five-to eight-week-old C57BL/6J male mice were bred and housed in the animal housing facilities at the University of Eastern Finland (Kuopio, Finland) and kept under specific-pathogen-free conditions in individually ventilated cages (1—4 mice/cage) under a 12/12 h light cycle at 20.6 °C (±0.2 °C) with 55%

(±0.8%) humidity. The mice were handled in accordance with Finnish legislation and the Council of European Convention ETS 123 on the use of vertebrate animals for scientific purposes. The number of mice per group was calculated using "G*Power" program [20] as previously described [21]. Eighteen mice were fed with the American Lifestyle-Induced Obesity Syndrome (ALIOS) diet, HFD (TD06303, Harlan Teklad, Madison, WI) and high-fructose corn syrup equivalent (45% glucose and 55% fructose by weight) at 42 g/L in the drinking water for MASLD induction as described by Tetri et al. [22]. After fourteen weeks, all the MASLD-induced mice were switched to the standard rodent chow control diet (2016 Teklad global 16% protein rodent diets, Harlan Teklad, Madison, WI) and randomly separated into three different groups for seven weeks. During these seven weeks, mice were trained to voluntarily daily consume gelatine cubes containing *E. coli* Nissle (at the concentration of 10^9 CFU per cube) expressing aldafermin (EcNA, n = 6) and *E. coli* Nissle without hormone expression (EcN, n = 6). Further, six mice did not receive any bacterial treatment and were resorted only to the dietary change (CTRL) (Figure 1A).

2.5. Sample collection

Mice were fasted for 2 h before terminal anesthesia with intraperitoneal injection (starting at 2 mL/kg mouse body) of pentobarbital ("Mebunat vet", Orion Pharma, Espoo, Finland). Blood extraction by cardiac puncture and cardiac perfusion were performed. Plasma samples were immediately separated from the whole blood using Microtainer tubes according to manufacturer's instructions (Category number: 365986, Becton, Dickinson and Company, Franklin Lakes, NJ, USA), frozen in liquid nitrogen before being stored in −80 °C. Fecal samples were collected on the day before the mice sacrifice and evaluated for the presence of live *E. coli* Nissle 1917 strain in EcNA and in EcN control group. The body and liver weight were measured weekly and during sample collection, respectively. EcNA group was compared against CTRL and EcN using Kruskal—Wallis test and Dunn post-hoc tests for pairwise comparison between groups using R software version 3.6.3 and GraphPad Prism (version 9.2.0).

2.6. Magnetic resonance imaging

Magnetic resonance imaging was performed and adapted as previously described [21] after fourteen weeks of ALIOS diet to confirm the extent of fat accumulation in the liver as MASLD induction marker (data not shown). Magnetic resonance imaging was performed again at the end of the study after the seven weeks of intervention in EcNA (n = 3/group), EcN (n = 3/group), CTRL mouse group (n = 5/group) for evaluating EcNA efficacy. Mice were anesthetized with isoflurane (Piramal, Netherland) (5% induction, 1.5% maintenance). The percentage differences between the two timepoints in liver fat accumulation in the EcNA group was compared against the CTRL and EcN group using Kruskal—Wallis test and Dunn post-hoc test in R software version 3.6.3 and graphics realized using GraphPad Prism software (version 9.2.0).

2.7. Biochemical parameters

Plasma samples were separated from the whole blood, frozen in liquid nitrogen, and stored in −80 °C, diluted 1:3 with 0.9% NaCl and concentrations of ALT, AST, total cholesterol, HDL-C, LDL-C, triglycerides, and glucose were measured by the automated clinical chemistry analyzer Konelab Prime 60 (Thermo Fisher Scientific, Waltham, Massachusetts, United States). The biochemical parameters in the EcNA group were compared against those in the CTRL and EcN
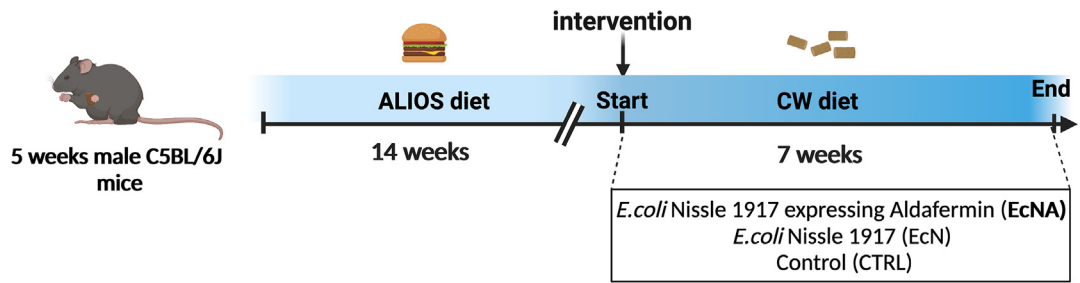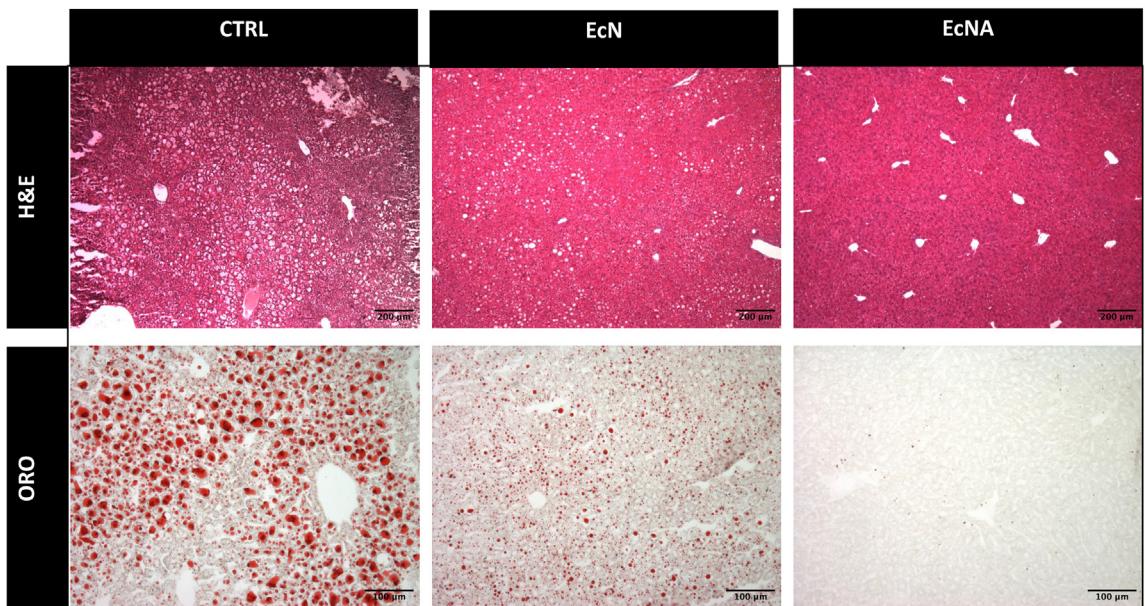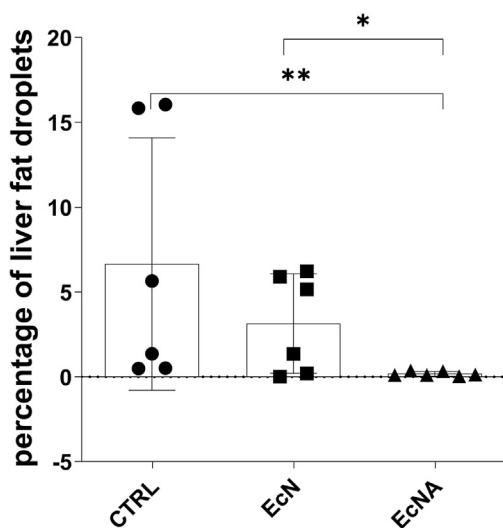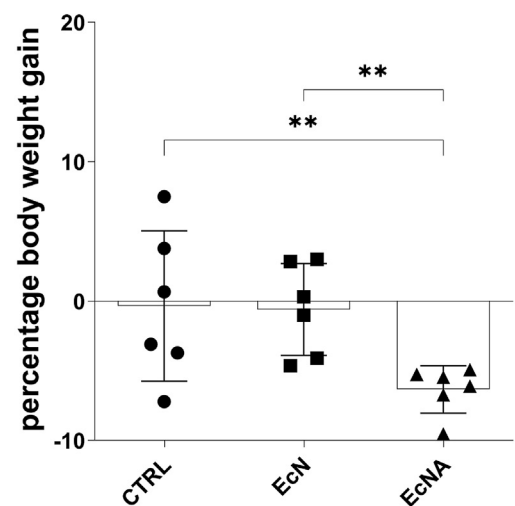
Figure 1: EcNA intervention reduced liver steatosis and body weight. A) Representation of the animal study intervention. B) Representative pictures of H&E and ORO staining after seven weeks of intervention. In H&E staining n = 6 mice/group, scale bar 200 μm, 4× objective. In ORO staining, the red droplets showed the fat droplets stained and accumulating in liver sections. n = 6 mice/group, 8 acquisitions/mouse, Scale bar 100 μm, 10× objective. C) Quantification of liver fat droplets as percentage of total fat in each tissue section 10× analyzed. n = 6 mice/group, 8 acquisitions/mouse, scale bar 100 μm, 10× objective. D) Percentage of body weight gain. n = 6 mice/all groups. Charts results of quantification of liver fat droplets and percentage of body weight gain were presented as average values where error bars denote SD. Statistical significance between different groups were shown using asterisks (*p ≤ 0.05 and **p ≤ 0.01). H&E: hematoxylin and eosin; ORO: Oil Red O.

group using Kruskal—Wallis test and Dunn post-hoc test in R software version 3.6.3 and graphics were realized using GraphPad Prism software (version 9.2.0).

2.8. Histology

The left lateral liver lobe was collected for Hematoxylin & Eosin staining as described [21]. Briefly, tissues were fixed overnight in 4% paraformaldehyde (VWR, Belgium, PFA) in Dulbecco's phosphate buffered saline $1\times$ (Thermo Fisher, Waltham, Massachusetts, United States, PBS) at 4 °C and stored in 70% ethanol at 4 °C until the processing. The samples were embedded into paraffin blocks and cut into 5 μm sections. Liver samples for Oil Red O staining (Sigma-Aldrich, Saint Louis, Missouri, USA) were fixed for 2 h in 4% PFA in PBS $1\times$, cryoprotected with a sucrose (Thermo Fisher, Waltham, Massachusetts, United States) scale (10% and 20% for 40 min and 30%) overnight in PBS $1\times$, included in OCT embedding medium (Thermo Fischer Scientific, Waltham, Massachussets, United States), frozen and stored at −80 °C. The samples were cut into 8 μm thick sections and stored at −80 °C. Hematoxylin (Bio-Optica, Milan, Italy) & Eosin (Bio-Optica, Milan, Italy) and Oil Red O (Sigma-Aldrich, Saint Louis, Missouri, USA) staining were performed in all mouse groups, and images were acquired using Olympus BX51 microscope (Olympus, Tokyo, Japan). Liver fat content in EcNA group was quantified using Fiji (ImageJ) software (version 1.52p) and trainable Weka Segmentation plugin [23] and compared against the control groups using Kruskal—Wallis test and Dunn post-hoc test using R software version 3.6.3 and GraphPad Prism software (version 9.2.0).

2.9. RNA-sequencing analysis

Liver tissues from all mice were collected and submersed in RNA stabilization solution (RNAprotect Tissue Reagent, Qiagen, Germany), frozen in liquid nitrogen and stored at −80 °C. The liver was homogenized in Buffer RLT (Cat. No./ID:79216, Qiagen, Germany) and extracted with RNeasy minikit (Qiagen, Germany). The RNase-free DNase I (Qiagen, Germany) treatment was performed for removing genomic DNA contaminants. RNA purity was checked using the NanoPhotometer® spectrophotometer (IMPLEN, CA, USA). RNA integrity and quantification was assessed using RNA Nano 6000 Assay Kit of the Bioanalyzer 2100 system (Agilent Technologies, CA, USA). Five mice per group were selected for transcriptome sequencing analysis based on the RNA purity (OD260/280 $\geq$ 2.0, OD260/230 $\geq$ 1.8) and quality (RIN $\geq$ 8.60). For sequencing library preparation 1 μg RNA per sample was used generated using NEBNext® UltraTM RNA Library Prep Kit for Illumina® (NEB, USA) following the manufacturer's recommendations. The library was then quantified using Qubit® 2.0 (Thermo Fisher, Waltham, Massachusetts, United State) and real-time PCR and the library quality was assessed with the Agilent Bioanalyzer 2100 system. The clustering of the index-coded samples was performed on a cBot Cluster Generation System using PE Cluster Kit cBot-HS (Illumina) according to the manufacturer's instructions. After cluster generation, the library preparations were sequenced on the Illumina platform Novaseq 6000 and 150 non-stranded paired-end reads were generated.

2.10. Data processing of RNA-sequencing

Raw reads of FASTQ format were first processed through fastp. Reads with adapter contamination, poly-N sequences, with low quality nucleotides (Base Quality less than 5), with low uncertain nucleotides (N > 10%) were removed. At the same time, Q20, Q30, and GC content of the clean data were calculated. All the downstream analyses were based on clean data with high quality. Reference genome and gene model annotation files were downloaded from https://www.ensembl.org/index.html. Paired-end clean reads were mapped using the Spliced Transcripts Alignment to a Reference software [24]. R package Subread [25] and the FeatureCounts [26] software were used to count the read numbers mapped to each gene. Differential expression analysis for comparisons among samples (five biological replicates per condition) was performed using DESeq2 [27]. Prefiltering was applied and counts ≤10 were discarded, as well as approximate posterior estimation for GLM coefficients (apeglm) [28] was applied to the differential expression analysis. Genes with a p-value <0.05 were considered significantly differentially expressed.

2.11. Non-targeted metabolomics analysis

Non-targeted metabolomics analysis was conducted according to Klåvus et al. [29]. The frozen sections of the liver samples (n = 6/group) were homogenized using Bead Ruptor 24 Elite homogenizer (6 m/s at 0 ± 2 °C for 30 s) in 80% v/v aqueous HPLC grade methanol (500 μL per 100 mg of sample) followed by vertexing, centrifugation (10 min, 4 °C at $20,000 \times g$), filtration (Captiva ND filter plate 0.2 μm) by centrifuging at (5 min, 4 °C at $700 \times g$), and storage at 4 °C until analysis. The liquid chromatography-mass spectrometry analysis was performed using two systems. For reversed-phase liquid chromatography, Vanquish Flex UHPLC 238 system (Thermo Scientific, Bremen, Germany) coupled to high-resolution Orbitrap mass 239 spectrometry (Q Exactive Focus, Thermo Scientific, Bremen, Germany) was employed. Hydrophilic interaction liquid chromatography was performed on a 1290 Infinity Binary UPLC coupled with a 6540 UHD Accurate-Mass quadrupole 243 time-of-flight MS (Agilent Technologies, California, United States). For both analytical setups, the data was acquired in positive and negative electrospray ionization modes. At the end of the analysis, data-dependent MS2 was acquired for each mode. Pooled liver samples were injected at the beginning of the analysis and after every 12 samples for quality control. Further details on the liquid chromatography-mass spectrometry instrument set-up and MS/MS analyses are previously described [21]. MS-DIAL (Version 4.60) [30] was employed for automated peak picking and alignment. Data preprocessing and statistical analyses were conducted in R Software version 3.6.3. The features were normalized for analytical drift. Missing values were imputed using random forest imputation for features with low number of missing values (present in more than 20% of the quality control samples), relative standard deviation* (RSD*) below 20%, and dispersion ratio* (D-ratio*) below 40%. In addition, if either the RSD* or D-ratio* was above the threshold, the features were kept if their classic RSD, RSD* and basic D-ratio were all below 10%. RSD* and D-ratio* are robust, non-parametric alternatives for RSD and D-ratio, based on median and median absolute deviation instead of mean and standard deviation. Other features were flagged, imputed with a value of 0, and discarded for statistical analyses. Feature-wise Welch's t-tests between the study groups were computed. All features with raw p-value <0.05, MS/MS spectrum, and average peak area of >10,000 across the samples were annotated as previously described [21]. Further, the abundances of specific annotated metabolites in EcNA were compared to CTRL and EcN using Kruskal—Wallis test and Dunn post-hoc test using R software version 3.6.3 and GraphPad Prism software (version 9.2.0).

2.12. Transcriptomics and metabolomics data integration

Principal component analysis using FPKM (fragments per kilobase of transcript per million fragments mapped) gene values and good-quality metabolite features from five biological replicates per group (*i.e.* EcNA, EcN, and CTRL), was performed in R Software version 3.6.3. Volcano

plots of fold changes and p-values for the transcriptomics and metabolomics data were created using VolcaNoseR [31]. Canonical pathway enrichment of the differentially expressed genes and all Level 1 and Level 2 annotated metabolites from the two comparisons (EcNA vs CTRL and EcNA vs EcN) were conducted using Ingenuity Pathway Analysis software (Qiagen, Hilden, Germany, https://digitalinsights.qiagen.com/IPA). The input transcriptomics data consisted of the gene symbol, the fold change values of the genes (for each comparison), and its corresponding p-values. In the case of metabolomics data, the input consisted of the metabolite ID (HMDB, KEGG, Pubchem CID, or CAS registry number), the fold change values of the abundances from six replicates (for each comparison), and its corresponding p-values. Each gene symbol and metabolite ID was mapped to its corresponding gene and metabolite object in the Ingenuity Knowledge Base genes + endogenous chemicals database. A core analysis was performed for each dataset to identify the canonical pathways. Further, a comparison analysis was performed between the two datasets. The resulting heatmap was filtered at the canonical pathway level using Benjamini–Hochberg adjusted (BH) p-value <0.05 and z-score threshold 1.5. Further, the pathways that were uniquely differential in one comparison, but passed the threshold of BH p-value <0.05 in the other comparison were also selected (Table S1). Further, the genes and metabolites implicated in individual pathways were manually checked using Ingenuity Target Explorer (QIAGEN, Inc.).

3. RESULTS

3.1. Engineered aldafermin-producing *E. coli* Nissle had reduced growth rate compared to the wild type

To create advanced microbial therapeutics for MASLD, the aldafermin gene was cloned under a constitutive promoter for robust expression in the murine gastrointestinal tract and *in vitro* conditions [19]. The production of aldafermin by the *E. coli* Nissle strains is shown in Supplemental Figure S2A. Further, to correlate the growth behavior of the strain with the production of aldafermin, the growth rate of *E. coli* Nissle expressing aldafermin was determined as an indirect measure of cell fitness. Overexpression of aldafermin in the aforementioned construct resulted in a 55% growth defect compared to the control *E. coli* Nissle vehicle (Supplemental Figure S2B).

3.2. EcNA intervention reduced liver steatosis, body weight, AST, and cholesterol levels in the plasma

To assess the impact of advanced microbial therapeutics in ameliorating MASLD, *E. coli* Nissle expressing aldafermin was administered for seven weeks together with dietary changes in MASLD mouse model (Figure 1A). The presence of living *E. coli* Nissle strain in the mice intestine was confirmed in fecal samples of mice. *E. coli* Nissle strains (with or without expression of aldafermin) were recovered with a range between 10^4–10^8 CFU/g from fecal samples of all mice.

In order to assess the liver morphology and to quantify the hepatic lipid content, histological examinations were performed. EcNA treatment ameliorated hepatic steatosis compared to control groups receiving dietary changes in combination with *E. coli* Nissle without hormone production (EcN) and without any bacteria (CTRL) (Figure 1B). The observations by hematoxylin & eosin staining showed a preserved healthy structure of the liver tissue in the EcNA group section with an absence of lipid fat droplets compared to CTRL and EcN groups (Figure 1B). Hematoxylin & eosin staining observations were further confirmed by Oil Red O staining (Figure 1B). Quantitative analysis of the percentage of liver fat droplets in tissue sections showed a significant decrease of fat content in the EcNA group compared to both CTRL and

EcN group (Figure 1C). Histological examinations were further confirmed by magnetic resonance imaging analysis. The results showed a significant increase in the percentage of magnetic resonance imaging fat index difference in the EcNA group compared to CTRL ($p = 0.0306$) (Supplemental Figure S3A and B). In line with the reduction of fat accumulation in the liver, EcNA effectively reduced body weight compared to both the CTRL group ($p = 0.0064$) and the EcN group ($p = 0.0055$) (Figure. 1D), while no significant changes in liver weight were observed (Supplemental Figure S3C and D).

To evaluate the efficacy of EcNA in ameliorating MASLD, some of the common disease biomarkers were measured. EcNA intervention significantly decreased plasma levels of AST compared to CTRL ($p = 0.0116$) and EcN ($p = 0.0258$) (Figure 2A) but not ALT levels (Supplemental Figure S3E). The EcNA group also showed a decrease of total plasma cholesterol level compared to CTRL ($p = 0.0007$) and EcN ($p = 0.0227$) (Figure 2B). Specifically, both high-density lipoprotein (HDL-C) and low-density lipoprotein (LDL-C) showed a significant reduction in plasma levels after seven weeks of EcNA compared to CTRL ($p = 0.0019$ for HDL-C, $p = 0.0012$ for LDL-C) and to EcN ($p = 0.0350$ for HDL-C, $p = 0.0040$ for LDL-C) (Figure 2C,D). Plasma glucose levels showed no significant difference between EcNA, CTRL, and EcN (Supplemental S3F). EcNA exhibited higher levels of plasma triglycerides than CTRL ($p = 0.0418$), although no significant difference was observed compared to EcN (Supplemental Figure S3G).

3.3. EcNA intervention changed the hepatic transcriptomic and metabolomic profiles

The efficacy of EcNA intervention was further evaluated by RNA-sequencing and non-targeted metabolomics approaches. These analyses revealed changes in several areas of metabolism upon EcNA intervention compared to controls (Figure 3A,B, Supplemental Tables 1–3). At the gene expression level, significant changes in genes involved in the glutathione metabolism, oxidative stress, and fatty acid oxidation such as *Mgst3, Gclc, Cpt2* were found (Figure 3A, B and Supplemental Table 2). At the metabolite level, the intervention decreased the levels of amino acids (e.g. tryptophan, isoleucine, and valine), peptides (e.g. glutathione), and amino acid-derived gut microbiota and microbiota-host co-metabolites (e.g. kynurenic acid, indole propionic acid, and hippuric acid). In contrast, metabolomic analysis revealed that certain lipids including lysophosphatidylcholines (LPCs), lysophosphatidylethanolamines (LPEs), lysophosphatidylinositols, acylcarnitines, primary bile acids, and lipid-derived gut microbiota and microbiota-host co-metabolites such as LPC (15:0) and secondary bile acids were increased in the EcNA group relative to the EcN and CTRL groups (Figure 3B, Supplemental Table 3). In addition, significant changes in gene expression and metabolite levels in the EcN group compared to CTRL were observed highlighting the host impacts of the *E. coli* Nissle (Supplemental Figure S4).

Thereafter, by integrating the transcriptomics with metabolomics data, a clear separation of the EcNA group from the CTRL and EcN groups was observed using principal component analysis (Figure 3C). Further, the combined canonical pathway analysis of both transcriptomics and metabolomics data for the differentially expressed genes and metabolites obtained for EcNA compared to CTRL and EcN groups revealed upregulation of urea cycle and downregulation of pathways related to amino acid metabolism (isoleucine, valine, tryptophan degradation), lipid metabolism (fatty acid beta-oxidation I and superpathway of geranylgeranylphosphate biosynthesis I), and their related-receptor signaling pathways including liver X receptor (LXR)-retinoid X receptor (RXR) activation, nuclear factor E2-related factor 2 (Nrf2)-mediated oxidative stress response signaling pathway, and aryl hydrocarbon
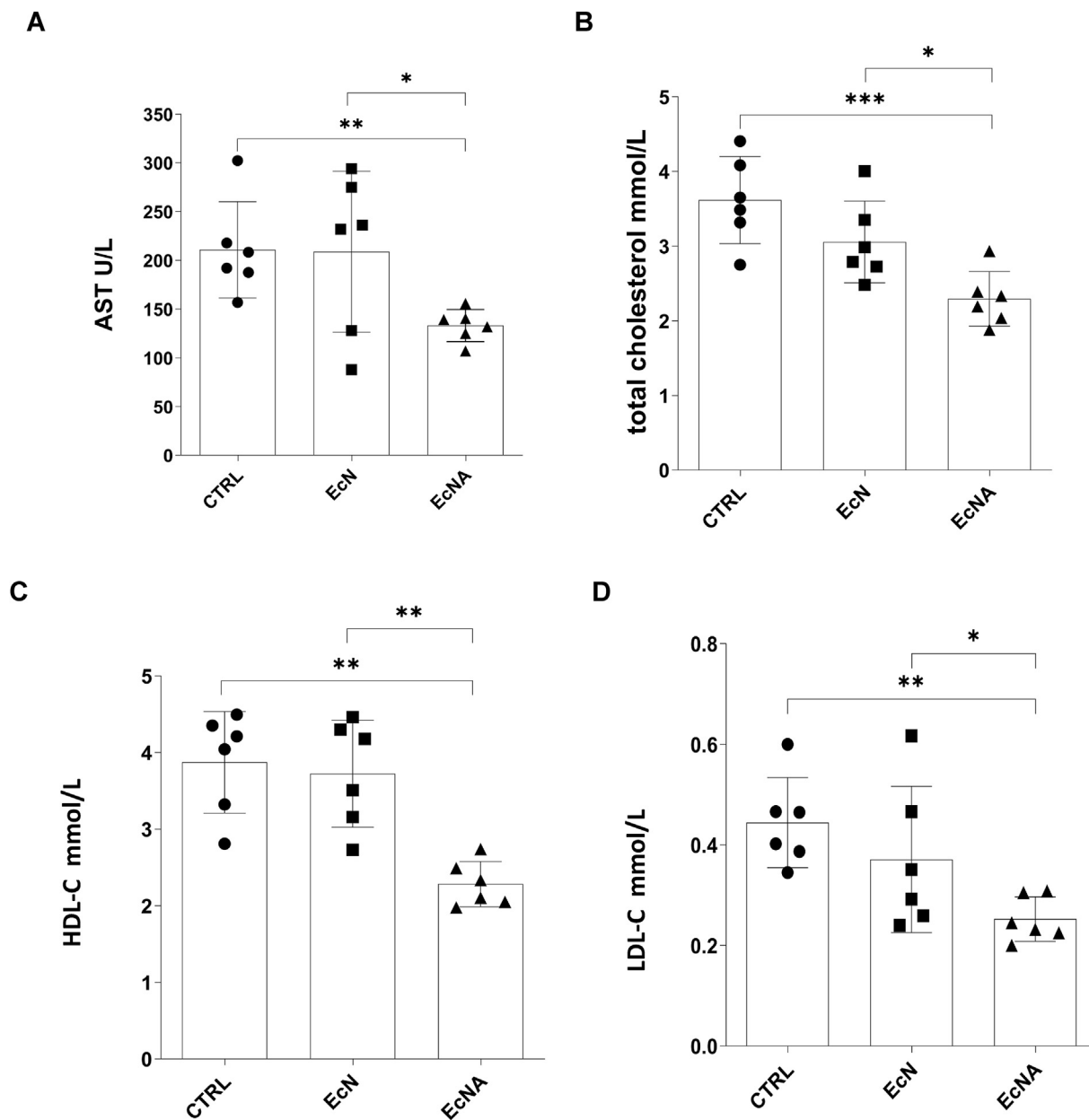
Figure 2: EcNA intervention reduced plasma biochemical markers after seven weeks of intervention. A) AST, B) total cholesterol, C) HDL-C, and D) LDL-C, n = 6 mice/all groups. Results are presented as average values. Error bars denote SD. Statistical significance between different groups were shown using asterisks (*p ≤ 0.05, **p ≤ 0.01, and ***p ≤ 0.001). AST: aspartate aminotransferase; HDL-C: high-density lipoprotein; LDL-C: low-density lipoprotein.

receptor (AHR) signaling pathway (Figures 3D, 4, 5, Supplemental Fig. S5, Supplemental Table S1).

4. DISCUSSION

This is the first study reporting the use of a novel genetically engineered *E. coli* Nissle 1917 expressing aldafermin in combination with dietary changes in MASLD mouse model, as non-invasive advanced microbial therapeutics for the disease.
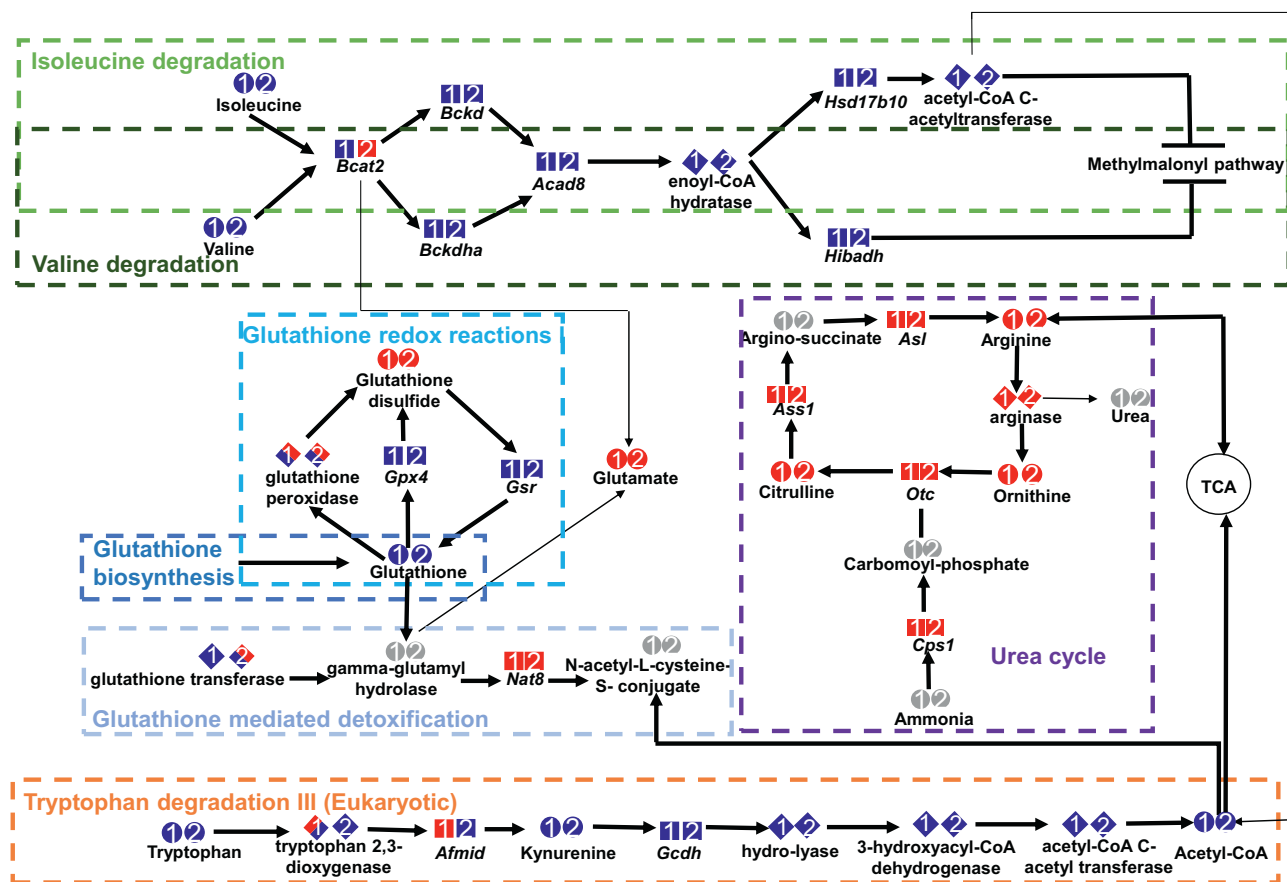
After MASLD induction, seven weeks of EcNA intervention reduced hepatic steatosis, body weight, AST, and plasma cholesterol levels (total cholesterol, HDL-C, and LDL-C) more effectively than either diet or EcN alone. By using transcriptomic and metabolomic profiling and

their combination in the liver, it was shown that the reduction of oxidative stress and improvement of insulin resistance (IR) could contribute to these observed physiological changes. Although aldafermin is an analog of FGF19 inhibiting bile acid synthesis from cholesterol [11], EcNA did not have a specific impact on the bile acid metabolism in the liver.

The beneficial effects of EcNA intervention in reducing the levels of plasma cholesterol were supported by the downregulation of the superpathway of geranylgeranyldiphosphate biosynthesis in the liver. This pathway is essential for cholesterol production in the liver and its downregulation might explain the reduced efflux of cholesterol to plasma. Additionally, these results were supported by the downregulation of LXR/RXR pathway, as its activation is shown to promote

Figure 3: EcNA intervention changed transcriptomic and metabolomic profiles in the liver. A) Volcano plots of differentially expressed genes for comparison between i) EcNA vs CTRL ii) EcNA vs EcN (n = 5/group). The data of all genes are plotted as log 2 (fold-change) versus the negative logarithm of the raw p-values. B) Volcano plots of annotated metabolites for comparison between i) EcNA vs CTRL. ii) EcNA vs EcN (n = 6/group). The data of all metabolites are plotted as log 2 (fold-change) versus the negative logarithm of the raw p-values. C) Principal component analysis of good quality metabolite features from untargeted metabolomics analysis and raw FPKM values from transcriptomics analysis (n = 5/group). D) Heatmap representing the comparative analysis of (EcNA vs CTRL) and (EcNA vs EcN) using Ingenuity pathway analysis (IPA). ACar — acylcarnitine, LPC — lysophosphatidylcholine, LPE — lysophosphatidylethanolamine, LPI — lysophosphatidylinositol, PC — phosphatidylcholine.

Figure 4: Pathways related to amino acid metabolism in EcNA group compared to CTRL (1), EcN (2). All annotated genes and metabolites are represented in the figure. Squares indicate genes, diamonds indicate gene complexes and circles indicate metabolites. Blue color implies downregulation, red implies upregulation, and gray implies unidentified genes or metabolites in our dataset. Thin lines represent by-products from the pathway. Direct and indirect associations between genes and metabolites in pathways are represented by arrows.
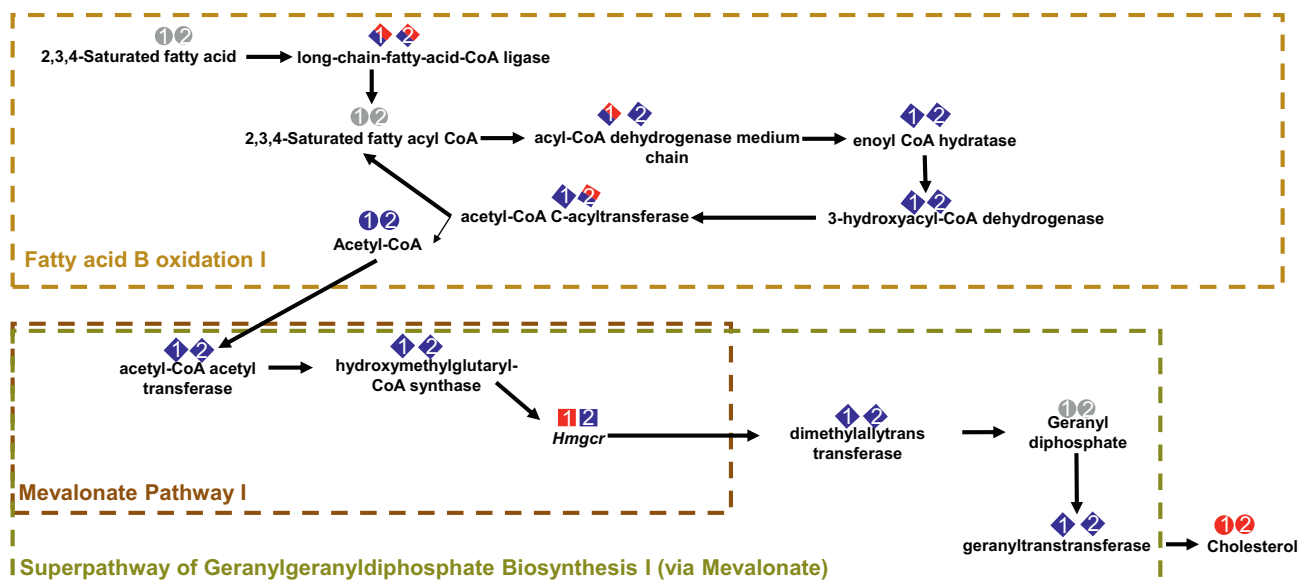
Figure 5: Pathways related to lipid metabolism in EcNA group compared to CTRL (1), EcN (2). All annotated genes and metabolites are represented in the figure. Squares indicate genes, diamonds indicate gene complexes, and circles indicate metabolites. Blue color implies downregulation, red implies upregulation, and gray implies unidentified genes or metabolites in our dataset. Thin lines represent by-products from the pathway. Direct and indirect associations between genes and metabolites in pathways are represented by arrows.

cholesterol efflux [32] and induce steatosis [33] as well as the increased levels of trigonelline in EcNA group.

In addition to reduced plasma cholesterol levels, previous interventions utilizing either genetically engineered *E. coli* Nissle producing bioactive molecules [12] or aldafermin alone [11] have also reported reduction in steatosis, body weight, and plasma AST, highlighting the potential of this novel EcNA modality to address hepatic diseases. Indeed, studies utilizing engineered *E. coli* Nissle expressing other bioactive molecules such as glucagon-like peptide 1 reported a reduction of body weight and hepatic steatosis in mice fed with HFD [17]. Further, genetically engineered *E. coli* Nissle producing N-acylphosphatidylethanolamines prevented steatosis and increased body weight in mice fed with HFD [18]. Similarly, Zhou et al., reported the reduction of hepatic steatosis and body weight after aldafermin treatment in high-fat, high-fructose, high-cholesterol diet (HFFCD)—induced nonalcoholic steatohepatitis mice [11]. The reduced body weight in this study is expected across all the study groups as the mice transitioned from a high-fat diet to the standard diet. The reduction in body weight across all groups could be attributed to the significant difference in energy content between the high-fat diet and the standard diet. Moreover, the ability of FGF19 in lowering the body weight has been attributed to its effect in increasing metabolic rate in the adipose tissue without significant changes in food intake [9,34]. Therefore, we may speculate that the specific reduction of body weight observed after EcNA intervention was possibly attributed to increased energy expenditure. However, the lack of confirmation by measuring the food intake represents a limitation in our study.

Due to the multifactorial origin of MASLD and its close association with metabolic disturbances, a combination of microbial therapeutics and dietary intervention was explored in this study. The observed changes in lipid and amino acid metabolism, along with their associated receptor signaling pathways, provide support for the potential beneficial effects of the EcNA intervention in reducing oxidative stress, steatosis, and IR. Notably, the EcNA intervention caused a significant decrease in the beta-oxidation pathway, possibly attributed to a reduction of fat accumulation in the liver [35]. Indeed, during MASLD, an excessive lipid accumulation in the liver is observed, leading to increased fatty acid oxidation and production of reactive oxygen species (ROS), which activate inflammation and oxidative stress [36]. Additionally, increased inflammation is associated with the activation of profibrotic hepatic stellate cells characterized by the increased production/secretion of extracellular matrix proteins and mitochondrial activity, including fatty acid oxidation [37]. However, the reversal of activated hepatic stellate cells into a quiescent-like healthy phenotype is associated with decreased mitochondrial activity [37]. Therefore, the EcNA intervention could attenuate MASLD-related oxidative stress likely by reducing beta oxidation, possibly influencing the bioenergetic signature of different liver cell types.

In the context of beta-oxidation, a significantly increased abundance of a majority of acylcarnitines in the liver of mice under EcNA intervention was also observed in this study. Acylcarnitines play a role as carriers to transport fatty acids into mitochondria for subsequent beta-oxidation [38]. Increased levels of acylcarnitines in the serum of patients with MASLD have been described [39]. However, the observed increase of several acylcarnitines in the liver of the EcNA group in this study might be attributed to the significantly reduced expression of *Cpt2* converting acylcarnitine to carnitine and entering beta-oxidation process, further supporting the downregulation of the beta-oxidation pathway. Therefore, these results support the potential role of EcNA in reducing ROS and alleviating oxidative stress.

The reduction of oxidative stress was further supported by the upregulation of the genes and metabolites involved in the urea cycle. This pathway plays a key role in detoxification of toxic compounds such as ammonia. High concentrations of ammonia enhance ROS production, further leading to MASLD progression [40]. Indeed, MASLD subjects have reduced expression of genes and proteins involved in the urea cycle, thereby causing an accumulation of ammonia [41]. In this study, the EcNA intervention resulted in an upregulation of the urea cycle, possibly promoting an increased excretion of ammonia in the form of urea and a decrease in the production of ROS.

The beneficial effects of the EcNA intervention in possibly reducing ROS was further evidenced by the decrease of glutathione, decreased expression of key genes related to oxidative stress response (*Mgst3, Gclc, and Nqo2*) [42], the downregulation of glutathione-associated pathways and NRF-2 mediated oxidative response signaling pathway. As oxidative stress is a pathological feature of MASLD, glutathione levels and *NRF2* are upregulated in MASLD [43,44]. The observed downregulation of these pathways could possibly imply reduced oxidative stress condition in the liver. Moreover, the depletion of glutathione in mice has been shown to prevent diet-induced obesity, improve insulin sensitivity, and regulate energy metabolism [45]. The decreased levels of glutathione and the downregulation of the glutathione-associated pathways suggest improvements to IR.

The downregulation of the isoleucine, valine, and tryptophan degradation pathways, together with the reduced expression of several key genes and lower abundance of metabolites in these pathways, provided further support for the enhancement of insulin sensitivity and decreased ROS production. The increased levels of tryptophan and branched chain amino acids (*i.e.* leucine, isoleucine, and valine) and the genes involved in their metabolism in the liver and in circulation were reported in MASLD as well as with the development of IR [46—51]. Further, the increased levels of a tryptophan metabolite, kynurenine, is associated with an increase of intrahepatic lipid accumulation [52]; and its subsequent activation of the AHR signaling, results in increased body weight, steatosis, and hyperglycemia in mice [53]. Moreover, tryptophan treatment in mice fed with high fructose-HFD is also known to induce ROS production [48]. In addition, the branched chain amino acids have been shown to induce IR in the liver involving the key pathways that are involved in glucose synthesis fueled by the mitochondria, housing the tricarboxylic acid cycle, which is closely coupled to mitochondrial respiration and ATP synthesis contributing to the generation of ROS [47]. Therefore, the observed downregulation of the tryptophan and branched chain amino acids pathways after EcNA intervention might confer beneficial effects in the context of MASLD.

The increased levels of LPC (15:0), a metabolite of potential gut-microbial origin which offers protection from diabetes by inducing insulin secretion and reducing glucose levels [54] decreased in HFD-fed mice [21] may further suggest a decrease of IR in this study, thereby inhibiting MASLD progression. In addition, the decreased levels of other gut-derived metabolites including indole propionic acid and hippuric acid might suggest the modulation of the gut—liver axis homeostasis and MASLD alleviation after EcNA intervention. Changes in other glycerophospholipids such as the increased levels of LPC (22:1) which is known to be decreased in mice fed with HFD [55], respectively, and a decrease of lysophosphatidylinositol (20:4), which is increased in the plasma of obese subjects [56], further support the beneficial effects of EcNA in MASLD. Furthermore, the EcNA intervention decreased PC (18:0/20:4), a potential biomarker to predict ethionamide-induced hepatic steatosis in rats [57]. Nevertheless, the role of other significantly changed lipids such as LPE (17:0), LPE (17:1),

and LPE (18:0) need to be further investigated in the context of MASLD. Improvements in pathway analysis tools aiming at increasing the coverage of lipids could enable the mapping of identified lipids to different pathways of biological significance.

In our study, we successfully produced aldafermin *in vitro*, but faced limitations when detecting it in plasma samples. Due to the short half-life of FGF19 (<30 min) [58], we speculate that the peptide might have degraded rapidly, or its levels might have been below the ELISA kit's detection limit. This may be due to the fact that our blood collection method, through cardiac puncture, may not be ideal for aldafermin detection. Future studies should consider more sensitive approaches such as high-performance liquid chromatography [59], and measurement of aldafermin levels from the gut content, liver, and portal vein. However, collecting blood from the portal vein might result in significantly lower amounts of blood sample, which may further pose challenges for conducting other analyses. Therefore, this represents a gap in our study since plasma levels of aldafermin might predict a direct link between the gut and liver axis and an important marker showing the effectiveness of EcNA intervention. Nevertheless, despite these technical limitations, we believe our approach was able to directly investigate aldafermin's downstream effects in various tissues of the mice and further validate the impact of aldafermin in alleviating MASLD.

5. CONCLUSIONS

In this study, a novel approach was employed to treat MASLD using an engineered *E. coli* Nissle 1917 strain that expresses aldafermin, in combination with dietary changes. Results showed that the treatment reduced body weight, hepatic steatosis, plasma total cholesterol, LDL-C, HDL-C, and AST in mice. Transcriptomics and metabolomics analyses revealed beneficial changes in amino acid and lipid metabolism, as well as associated receptor signaling pathways, which are associated with improved hepatic steatosis, oxidative stress, and IR in the MASLD mouse model. The intervention also showed beneficial effects on metabolites of possible gut microbial origin. The promising results of this study highlight the potential of EcNA as a therapeutic candidate for not only inhibiting MASLD progression but also potentially treating other multifactorial diseases. With further research, EcNA could pave the way for a new generation of microbial therapeutics that tackle complex metabolic disorders.

AUTHOR CONTRIBUTIONS

The authors confirm contribution to the paper as follows: study conception and design: V.I., J.L., C.G.G., R.V.U., T.H.V., M.B., M.O.A.S., M. Kolehmainen, and H.N. Data collection: V.I., J.L., A.F.B., C.G.G., and I.T. Analysis and interpretation of results: V.I., A.F.B., C.G.G., G.D., J.L., M. Kettunen, A. K., S.K., R.S., D.K., J.P., R.V.U., M.O.A.S., K.H., H.N, and M. Kolehmainen. Draft manuscript preparation: V.I. and A.F.B. drafted the first version of the manuscript under the supervision of C.G.G., K.H., H.N., and M.Kolehmainen. All authors read, reviewed, and approved the final manuscript.

DECLARATION OF COMPETING INTEREST

The authors declare that they have no known competing financial interests or personal relationships that could have appeared to influence the work reported in this paper.

DATA AVAILABILITY

RNA-sequencing data have been deposited with accession number GSE232030 in NCBI's Gene Expression Omnibus 60. R codes used for metabolomics data processing and statistical analyses are available online.

APPENDIX A. SUPPLEMENTARY DATA

Supplementary data to this article can be found online at https://doi.org/10.1016/j.molmet.2023.101823.

REFERENCES

[1] Tiniakos DG, Vos MB, Brunt EM. Nonalcoholic fatty liver disease: pathology and pathogenesis. Annu Rev Pathol Mech Dis 2010;5(1):145–71. https://doi.org/10.1146/annurev-pathol-121808-102132.

[2] Friedman SL, Neuschwander-Tetri BA, Rinella M, Sanyal AJ. Mechanisms of NAFLD development and therapeutic strategies. Nat Med 2018;24(7):908–22. https://doi.org/10.1038/s41591-018-0104-9.

[3] Chen Z, Yu R, Xiong Y, Du F, Zhu S. A vicious circle between insulin resistance and inflammation in nonalcoholic fatty liver disease. Lipids Health Dis 2017;16(1):203. https://doi.org/10.1186/s12944-017-0572-9.

[4] Chen Z, Tian R, She Z, Cai J, Li H. Role of oxidative stress in the pathogenesis of nonalcoholic fatty liver disease. Free Radic Biol Med 2020;152:116–41. https://doi.org/10.1016/j.freeradbiomed.2020.02.025.

[5] Yamaguchi K, Yang L, McCall S, Huang J, Yu XX, Pandey SK, et al. Inhibiting triglyceride synthesis improves hepatic steatosis but exacerbates liver damage and fibrosis in obese mice with nonalcoholic steatohepatitis. Hepatology 2007;45(6):1366–74. https://doi.org/10.1002/hep.21655.

[6] Hirsova P, Ibrabim SH, Gores GJ, Malhi H. Lipotoxic lethal and sublethal stress signaling in hepatocytes: relevance to NASH pathogenesis. J Lipid Res 2016;57(10):1758–70. https://doi.org/10.1194/jlr.R066357.

[7] Schreuder TCMA, Marsman HA, Lenicek M, van Werven JR, Nederveen AJ, Jansen PLM, et al. The hepatic response to FGF19 is impaired in patients with nonalcoholic fatty liver disease and insulin resistance. Am J Physiol Gastrointest Liver Physiol 2010;298(3):G440–5. https://doi.org/10.1152/ajpgi.00322.2009.

[8] Degirolamo C, Sabbà C, Moschetta A. Therapeutic potential of the endocrine fibroblast growth factors FGF19, FGF21 and FGF23. Nat Rev Drug Discov 2016;15(1):51–69. https://doi.org/10.1038/nrd.2015.9.

[9] Fu L, John LM, Adams SH, Yu XX, Tomlinson E, Renz M, et al. Fibroblast growth factor 19 increases metabolic rate and reverses dietary and leptin-

deficient diabetes. Endocrinology 2004;145(6):2594—603. https://doi.org/10.1210/en.2003-1671.

[10] Zhou M, Wang X, Phung V, Lindhout DA, Mondal K, Hsu J-Y, et al. Separating tumorigenicity from bile acid regulatory activity for endocrine hormone FGF19. Cancer Res 2014;74(12):3306—16. https://doi.org/10.1158/0008-5472.CAN-14-0208.

[11] Zhou M, Learned RM, Rossi SJ, DePaoli AM, Tian H, Ling L. Engineered FGF19 eliminates bile acid toxicity and lipotoxicity leading to resolution of steatohepatitis and fibrosis in mice: Zhou et al. Hepatol Commun 2017;1(10):1024—42. https://doi.org/10.1002/hep4.1108.

[12] Harrison SA, Neff G, Guy CD, Bashir MR, Paredes AH, Frias JP, et al. Efficacy and safety of aldafermin, an engineered FGF19 analog, in a randomized, double-blind, placebo-controlled trial of patients with nonalcoholic steatohepatitis. Gastroenterology 2021;160(1):219—231.e1. https://doi.org/10.1053/j.gastro.2020.08.004.

[13] Lang S, Schnabl B. Microbiota and fatty liver disease—the known, the unknown, and the future. Cell Host Microbe 2020;28(2):233—44. https://doi.org/10.1016/j.chom.2020.07.007.

[14] Aron-Wisnewsky J, Vigliotti C, Witjes J, Le P, Holleboom AG, Verheij J, et al. Gut microbiota and human NAFLD: disentangling microbial signatures from metabolic disorders. Nat Rev Gastroenterol Hepatol 2020;17(5):279—97. https://doi.org/10.1038/s41575-020-0269-9.

[15] Castillo V, Figueroa F, González-Pizarro K, Jopia P, Ibacache-Quiroga C. Probiotics and prebiotics as a strategy for non-alcoholic fatty liver disease, a narrative review. Foods 2021;10(8):1719. https://doi.org/10.3390/foods10081719.

[16] Hany NM, Eissa S, Basyouni M, Hasanin AH, Aboul-Ela YM, Elmagd NMA, et al. Modulation of hepatic stellate cells by Mutaflor® probiotic in non-alcoholic fatty liver disease management. J Transl Med 2022;20(1):342. https://doi.org/10.1186/s12967-022-03543-z.

[17] Ma J, Li C, Wang J, Gu J. Genetically engineered *Escherichia coli* Nissle 1917 secreting GLP-1 analog exhibits potential antiobesity effect in high-fat diet-induced obesity mice. Obesity 2020;28(2):315—22. https://doi.org/10.1002/oby.22700.

[18] Chen Z, Guo L, Zhang Y, L. Walzem R, Pendergast JS, Printz RL, et al. Incorporation of therapeutically modified bacteria into gut microbiota inhibits obesity. J Clin Investig 2014;124(8):3391—406. https://doi.org/10.1172/JCI72517.

[19] Armetta J, Schantz-Klausen M, Shepelin D, Vazquez-Uribe R, Bahl MI, Laursen MF, et al. Escherichia coli promoters with consistent expression throughout the murine gut. ACS Synth Biol 2021;10(12):3359—68. https://doi.org/10.1021/acssynbio.1c00325.

[20] Faul F, Erdfelder E, Buchner A, Lang A-G. Statistical power analyses using G*Power 3.1: tests for correlation and regression analyses. Behav Res Methods 2009;41(4):1149—60. https://doi.org/10.3758/BRM.41.4.1149.

[21] Iannone V, Babu AF, Gómez-Gallego C, Willman RM, Koistinen VM, Klåvus A, et al. Associations of altered hepatic gene expression in American lifestyle-induced obesity syndrome diet-fed mice with metabolic changes during NAFLD development and progression. J Nutr Biochem 2023:109307. https://doi.org/10.1016/j.jnutbio.2023.109307.

[22] Tetri LH, Basaranoglu M, Brunt EM, Yerian LM, Neuschwander-Tetri BA. Severe NAFLD with hepatic necroinflammatory changes in mice fed trans fats and a high-fructose corn syrup equivalent. Am J Physiol Gastrointest Liver Physiol 2008;295(5):G987—95. https://doi.org/10.1152/ajpgi.90272.2008.

[23] Arganda-Carreras I, Kaynig V, Rueden C, Eliceiri KW, Schindelin J, Cardona A, et al. Trainable Weka Segmentation: a machine learning tool for microscopy pixel classification. Bioinformatics 2017;33(15):2424—6. https://doi.org/10.1093/bioinformatics/btx180.

[24] Dobin A, Davis CA, Schlesinger F, Drenkow J, Zaleski C, Jha S, et al. STAR: ultrafast universal RNA-seq aligner. Bioinformatics 2013;29(1):15—21. https://doi.org/10.1093/bioinformatics/bts635.

[25] Liao Y, Smyth GK, Shi W. The R package Rsubread is easier, faster, cheaper and better for alignment and quantification of RNA sequencing reads. Nucleic Acids Res 2019;47(8). https://doi.org/10.1093/nar/gkz114. e47—e47.

[26] Liao Y, Smyth GK, Shi W. featureCounts: an efficient general purpose program for assigning sequence reads to genomic features. Bioinformatics 2014;30(7):923—30. https://doi.org/10.1093/bioinformatics/btt656.

[27] Love MI, Huber W, Anders S. Moderated estimation of fold change and dispersion for RNA-seq data with DESeq2. Genome Biol 2014;15(12):550. https://doi.org/10.1186/s13059-014-0550-8.

[28] Zhu A, Ibrahim JG, Love MI. Heavy-tailed prior distributions for sequence count data: removing the noise and preserving large differences. Bioinformatics 2019;35(12):2084—92. https://doi.org/10.1093/bioinformatics/bty895.

[29] Klåvus A, Kokla M, Noerman S, Koistinen VM, Tuomainen M, Zarei I, et al. "Notame": workflow for non-targeted LC—MS metabolic profiling. Metabolites 2020;10(4):135. https://doi.org/10.3390/metabo10040135.

[30] Tsugawa H, Cajka T, Kind T, Ma Y, Higgins B, Ikeda K, et al. MS-DIAL: data-independent MS/MS deconvolution for comprehensive metabolome analysis. Nat Methods 2015;12(6):523—6. https://doi.org/10.1038/nmeth.3393.

[31] Goedhart J, Luijsterburg MS. VolcaNoseR is a web app for creating, exploring, labeling and sharing volcano plots. Sci Rep 2020;10(1):20560. https://doi.org/10.1038/s41598-020-76603-3.

[32] Lee SD, Tontonoz P. Liver X receptors at the intersection of lipid metabolism and atherogenesis. Atherosclerosis 2015;242(1):29—36. https://doi.org/10.1016/j.atherosclerosis.2015.06.042.

[33] Ahn SB, Jang K, Jun DW, Lee BH, Shin KJ. Expression of liver X receptor correlates with intrahepatic inflammation and fibrosis in patients with nonalcoholic fatty liver disease. Dig Dis Sci 2014;59(12):2975—82. https://doi.org/10.1007/s10620-014-3289-x.

[34] Antonellis PJ, Droz BA, Cosgrove R, O'Farrell LS, Coskun T, Perfield JW, et al. The anti-obesity effect of FGF19 does not require UCP1-dependent thermogenesis. Mol Metab 2019;30:131—9. https://doi.org/10.1016/j.molmet.2019.09.006.

[35] Ma Y, Lee G, Heo S-Y, Roh Y-S. Oxidative stress is a key modulator in the development of nonalcoholic fatty liver disease. Antioxidants 2021;11(1):91. https://doi.org/10.3390/antiox11010091.

[36] Zisser A, Ipsen DH, Tveden-Nyborg P. Hepatic stellate cell activation and inactivation in NASH-fibrosis—roles as putative treatment targets? Biomedicines 2021;9(4):365. https://doi.org/10.3390/biomedicines9040365.

[37] Gajendiran P, Vega LI, Itoh K, Sesaki H, Vakili MR, Lavasanifar A, et al. Elevated mitochondrial activity distinguishes fibrogenic hepatic stellate cells and sensitizes for selective inhibition by mitotropic doxorubicin. J Cell Mol Med 2018;22(4):2210—9. https://doi.org/10.1111/jcmm.13501.

[38] Schooneman MG, Vaz FM, Houten SM, Soeters MR. Acylcarnitines. Diabetes 2013;62(1):1—8. https://doi.org/10.2337/db12-0466.

[39] Enooku K, Nakagawa H, Fujiwara N, Kondo M, Minami T, Hoshida Y, et al. Altered serum acylcarnitine profile is associated with the status of nonalcoholic fatty liver disease (NAFLD) and NAFLD-related hepatocellular carcinoma. Sci Rep 2019;9(1):10663. https://doi.org/10.1038/s41598-019-47216-2.

[40] Jalan R, De Chiara F, Balasubramaniyan V, Andreola F, Khetan V, Malago M, et al. Ammonia produces pathological changes in human hepatic stellate cells and is a target for therapy of portal hypertension. J Hepatol 2016;64(4):823—33. https://doi.org/10.1016/j.jhep.2015.11.019.

[41] De Chiara F, Heebøll S, Marrone G, Montoliu C, Hamilton-Dutoit S, Ferrandez A, et al. Urea cycle dysregulation in non-alcoholic fatty liver disease. J Hepatol 2018;69(4):905—15. https://doi.org/10.1016/j.jhep.2018.06.023.

[42] Cazanave S, Podtelezhnikov A, Jensen K, Seneshaw M, Kumar DP, Min H-K, et al. The transcriptomic signature of disease development and progression of nonalcoholic fatty liver disease. Sci Rep 2017;7(1):17193. https://doi.org/10.1038/s41598-017-17370-6.

[43] Yang S, Zhu H, Li Y, Lin H, Gabrielson K, Trush MA, et al. Mitochondrial adaptations to obesity-related oxidant stress. Arch Biochem Biophys 2000;378(2):259—68. https://doi.org/10.1006/abbi.2000.1829.

[44] Mohs A, Otto T, Schneider KM, Peltzer M, Boekschoten M, Holland CH, et al. Hepatocyte-specific NRF2 activation controls fibrogenesis and carcinogenesis in steatohepatitis. J Hepatol 2021;74(3):638—48. https://doi.org/10.1016/j.jhep.2020.09.037.

[45] Findeisen HM, Gizard F, Zhao Y, Qing H, Jones KL, Cohn D, et al. Glutathione depletion prevents diet-induced obesity and enhances insulin sensitivity. Obesity 2011;19(12):2429—32. https://doi.org/10.1038/oby.2011.298.

[46] Chen T, Zheng X, Ma X, Bao Y, Ni Y, Hu C, et al. Tryptophan predicts the risk for future type 2 diabetes. PLoS One 2016;11(9):e0162192. https://doi.org/10.1371/journal.pone.0162192.

[47] Sunny NE, Kalavalapalli S, Bril F, Garrett TJ, Nautiyal M, Mathew JT, et al. Cross-talk between branched-chain amino acids and hepatic mitochondria is compromised in nonalcoholic fatty liver disease. Am J Physiol Endocrinol Metab 2015;309(4):E311—9. https://doi.org/10.1152/ajpendo.00161.2015.

[48] Osawa Y, Kanamori H, Seki E, Hoshi M, Ohtaki H, Yasuda Y, et al. I-Tryptophan-mediated enhancement of susceptibility to nonalcoholic fatty liver disease is dependent on the mammalian target of rapamycin. J Biol Chem 2011;286(40):34800—8. https://doi.org/10.1074/jbc.M111.235473.

[49] Mello VD, Sehgal R, Männistö V, Klåvus A, Nilsson E, Perfilyev A, et al. Serum aromatic and branched-chain amino acids associated with NASH demonstrate divergent associations with serum lipids. Liver Int 2021;41(4):754—63. https://doi.org/10.1111/liv.14743.

[50] Lake AD, Novak P, Shipkova P, Aranibar N, Robertson DG, Reily MD, et al. Branched chain amino acid metabolism profiles in progressive human nonalcoholic fatty liver disease. Amino Acids 2015;47(3):603—15. https://doi.org/10.1007/s00726-014-1894-9.

[51] Toye AA, Dumas ME, Blancher C, Rothwell AR, Fearnside JF, Wilder SP, et al. Subtle metabolic and liver gene transcriptional changes underlie diet-induced fatty liver susceptibility in insulin-resistant mice. Diabetologia 2007;50(9):1867—79. https://doi.org/10.1007/s00125-007-0738-5.

[52] Sui G, Jia L, Quan D, Zhao N, Yang G. Activation of the gut microbiota-kynurenine-liver axis contributes to the development of nonalcoholic hepatic steatosis in nondiabetic adults. Aging 2021;13(17):21309—24. https://doi.org/10.18632/aging.203460.

[53] Rojas IY, Moyer BJ, Ringelberg CS, Wilkins OM, Pooler DB, Ness DB, et al. Kynurenine-induced aryl hydrocarbon receptor signaling in mice causes body mass gain, liver steatosis, and hyperglycemia. Obesity 2021;29(2):337—49. https://doi.org/10.1002/oby.23065.

[54] de Mello VD, Selander T, Lindström J, Tuomilehto J, Uusitupa M, Kaarniranta K. Serum levels of plasmalogens and fatty acid metabolites associate with retinal microangiopathy in participants from the Finnish diabetes prevention study. Nutrients 2021;13(12):4452. https://doi.org/10.3390/nu13124452.

[55] Cheng L, Zhang S, Shang F, Ning Y, Huang Z, He R, et al. Emodin improves glucose and lipid metabolism disorders in obese mice via activating Brown adipose tissue and inducing browning of white adipose tissue. Front Endocrinol 2021;12:618037. https://doi.org/10.3389/fendo.2021.618037.

[56] Moreno-Navarrete JM, Catalán V, Whyte L, Díaz-Arteaga A, Vázquez-Martínez R, Rotellar F, et al. The l-α-Lysophosphatidylinositol/GPR55 system and its potential role in human obesity. Diabetes 2012;61(2):281—91. https://doi.org/10.2337/db11-0649.

[57] Muta K, Saito K, Kemmochi Y, Masuyama T, Kobayashi A, Saito Y, et al. Phosphatidylcholine (18:0/20:4), a potential biomarker to predict ethionamide-induced hepatic steatosis in rats. J Appl Toxicol 2022;42(9):1533—47. https://doi.org/10.1002/jat.4324.

[58] Avalos-de León CG, Jiménez-Castro MB, Cornide-Petronio ME, Gulfo J, Rotondo F, Gracia-Sancho J, et al. The effect of fibroblast growth factor 15 signaling in non-steatotic and steatotic liver transplantation from cardiocirculatory death. Cells 2019;8(12):1640. https://doi.org/10.3390/cells8121640.

[59] Honour JW. Gas chromatography-mass spectrometry. In: Wheeler MJ, Hutchinson JSM, editors. Hormone assays in biological fluids. Totowa, NJ: Humana Press; 2006. p. 53—74.

[60] Edgar R. Gene Expression Omnibus: NCBI gene expression and hybridization array data repository. Nucleic Acids Res 2002;30(1):207—10. https://doi.org/10.1093/nar/30.1.207.